Research article

Kinetic triplet of Colombian sawmill wastes using thermogravimetric analysis

Javier Bonilla [*], Robert Paul Salazar, Manuel Mayorga

Grupo de Investigación de Aprovechamiento Tecnológico de Materiales y Energía, GIATME, Universidad ECCI, Cra. 19 No. 49-20, Bogotá, Código Postal 111311, Colombia

A R T I C L E   I N F O

A B S T R A C T

The potential of sawmill wastes as a raw material in pyrolysis process is presented in this study. Non-isothermal thermogravimetric analysis (TGA and DTG) and isoconversional methods were employed to determine triplet kinetic (activation energy, reaction model and pre-exponential factor). Through TGA and DTG, the conversion degree is described as a function of temperature for five heating rates (10, 20, 30, 40 and 50° C/min) and four model-free methods (Flynn-Wall-Ozawa (FWO), Kissinger-Akahira-Sunose (KAS), Friedman, and Vyazovkin) with temperatures ranging from 25 to 1000°C were employed. Isoconversional lines were built for every method at different isoconversional degrees $\alpha \in [0,1]$. The activation energy E was found as a function of α in the interval $\chi_{II} = [0.2, 0.7]$ where each isoconversional methods were in agreement and the estimated error was sufficiently small. Findings show the same activation energy profile independently of the isoconversional method. In particular the total variation of E in χ_{II} was as follows: 209.909–228.238 kJ/mol (FWO); 211.235–229.277 kJ/mol (KAS); 223.050–188.512 kJ/mol (Friedman), and 211.449 kJ/mol-229.512 kJ/mol (Vyazovkin). The reaction model of the process in χ_{II} matched with a two-dimensional diffusion (D_2) by using a master-plot analysis. The calculated and reported parameters are fundamental information for the pyrolysis reactor design using Sawmill wastes as feedstock.

1. Introduction

The development of cutting-edge technologies based on thermochemical processes for the transformation of second-generation feedstock into competitive biofuels has led to study new raw materials [1, 2, 3, 4, 5, 6, 7, 8, 9, 10]. Biomass belongs to this kind of feedstock and previous research have confirmed many advantages on raw material to be converted via pyrolysis [11, 12, 13, 14, 15, 16, 17, 18, 19, 20]. In addition, pyrolysis is a suitable process to transform lignocellulosic biomass since most of its compounds can be converted into fuel-products easier and faster compared to non-thermochemical processes such as biodigestion, biological conversion, and chemical conversion [21, 22, 23, 24, 25, 26]. Pyrolysis is defined as the thermochemical process where the decomposition of organic materials occurs, obtaining a range of useful products such as gas, liquid, and fixed carbon fuels yielded in an environment with no oxidizing sources at temperatures from 300 °C to 650 °C [27].

Sawmill wastes (SW) is a by-product of the wood-industrial sector which is used as mulch and fuel [11, 28]. Crops and production of wood are by 2% of Colombian GDP, composed of 361000 m^3 of wood waste,

915000 m^3 of pulpwood annual production and 114000 m^3 of SW [29]. Then, production of these biofuels would supply the thermal machines fed by gas and liquid fuels used in sawmills, mitigating the dependence on fossil fuels, and helping reduce the issues generated by waste mismanagement. Fast pyrolysis is a thermochemical process where organic material is carried out into an environment at a temperature around 500 °C during up to 2s, where up to 75% of the material is converted into liquid fuels [13].

Kinetic and thermodynamic parameters, as well as the reaction mechanisms, take relevance in the modeling, testing, and design of reactors involving the conversion of biomass throughout the pyrolysis process. An analysis that helps understand the pyrolysis process is the TGA, not only because it may approximate the pyrolysis process, but also the TGA analysis has been effectively proven as the main method to study the pyrolysis kinetic performance [2, 16, 20, 30]. In this work, we present an analysis of the TGA and DTG results obtained for SW. This document also presents a computation of the activation energy according to the recommendations published by The International Confederation of Thermal Analysis and Calorimetry (ICTAC) in [31, 32], where

---

isoconversional methods based on non-isothermal model-free are suggested to study lignocellulosic biomasses. The ICTAC recommendations take into account that constituents of such biomasses decompose at different temperatures and reactions generated over there are complex, which means that the triplet kinetic varies with the temperature.

Although several research have been presented about behavior of pyrolysis of biomass via modelling of particles [33, 34, 35], it is recognized that every biomass in nature has both a particular and unique behavior when submitting in an thermochemical process like pyrolysis. Thus, TGA has been one of the most used methods to represent pyrolysis due to similar environmental experimental conditions of the biomass in this kind of reactors. Moreover, in spite of TGA is more linked to single lumped reaction, many studies support that obtained results from TGA via model-free analysis are very similar compared to those of pyrolysis reactors in experimental studies for large biomass samples. Thereby, isoconversional non-isothermal methods can provide kinetic parameters for design of reactors as shown in [36, 37, 38, 39].

Thus, in this work, four different methods were employed: Flynn-Wall-Ozawa (FWO), Kissinger-Akahira-Sunose (KAS), Friedman, and the integral-based method reported by Vyazovkin [32]. The activation energy $E(\alpha)$ was calculated by using every method mentioned. Further, a master plot was built and later analysed to determine the reaction function $f(\alpha)$ and the model $g(\alpha)$ of the pyrolysis process. Then, once $f(\alpha)$ is found, the pre-exponential factor $A(\alpha)$ is calculated. Finally, a plot of $\log A$ vs α was built allowing to verify the activation energy $E(\alpha)$ and $f(\alpha)$.

2. Materials and methods

2.1. Materials

2.1.1. Sawmill waste

The SW samples were analyzed chemically through proximate and ultimate analysis. Firstly, the samples were treated following the requirements of ASTM D2013 standard. Then, the analyses of samples were carried out following the next standards: moisture analysis (ASTM D3302), ash content analysis (ASTM D3174), volatile matter (ASTM D3175/D7582), fixed carbon (ASTM D3172), sulphur analysis (ASTM D4239), higher heating value (ASTM D5865), carbon analysis, hydrogen and nitrogen (ASTM D5373), total sulfides (ASTM 2492) and elemental ash analysis (ASTM D3174-12/D7582-15). Finally, the cellulose content and lignin tests were performed under TAPPI T-203, TAPPI T-223, and ASTM D-1106 standards, respectively.

2.1.2. TGA tests

The thermochemical behavior of biomass was evaluated by TGA tests under pyrolysis conditions, following the ASTM E-1131 standard in non-isothermal conditions using a Mettler Toledo TGA 2 - XP1 equipment. TGA tests were performed several times on different SW samples (10 mg wt), at multiples constant heating rates (10, 20, 30, 40 and 50 °C/min) ranging from 25 °C to 1000 °C in an inert environment generated by a carrier gas (nitrogen 99.99 %) flow rate of 150 ml/min. The tests were carried out three times to evaluate its repeatability.

2.2. Non-isothermal model-free isoconversional methods

The isoconversional methods Flynn-Wall-Ozawa (FWO), Kissinger-Akahira-Sunose (KAS), Friedman and Vyazovkin were compared to determined different kinetic parameters that occurring throughout the pyrolysis process of SW.

2.2.1. Kinetic theory

The temporal change of the extent of conversion α in a system following a thermally stimulated process can be written in terms of the temperature T as follows

$$\frac{d\alpha}{dt} = k(T)f(\alpha)$$

where α is the grade of conversion, t is the time, $f(\alpha)$ is the reaction function and $k(T)$ is the decomposition rate constant

$$k(T) = A \ \exp\left(-\frac{E}{RT}\right)$$

which is provided by Arrhenius formulation where A $[s^{-1}]$ is the pre-exponential factor, $E = E(\alpha)$ [J/mol] is the activation energy, $R = 8.31446261815324$ J/(mol K) is the ideal gas constant and T is the reaction temperature [K]. In the current study, α is the volatile biomass fraction given by

$$\alpha(T) : = \frac{m_1 - m(T)}{m_1 - m_N}$$

where $m(T)$ is the solid-sample mass at the working temperature during TGA test, m_1 and m_N represent the initial and final solid-sample mass through pyrolysis process, respectively. Non-isothermal free-model methods are used to obtain the kinetics parameters and a non-isothermal TGA analysis is applied in this study with a constant increase of temperature β. This enables to write the kinetic equation as follows

$$\frac{d\alpha}{dT} = \frac{A_\alpha}{\beta} f(\alpha)\exp\left(-\frac{E}{RT}\right) \text{with} \ \ \beta = \frac{dT}{dt}. \tag{1}$$

The Eq. (1) plays an important role in the formulation of analytical methods since it allows to calculate kinetic parameters by using the non-isothermal TGA results. Frequently, the reaction function $f(\alpha)$ is unknown, then it is convenient to write Eq. (1) as follows

$$g(\alpha) = \int_0^\alpha \frac{d\alpha}{f(\alpha)} = \frac{A_\alpha}{\beta}. \int_0^T \exp\left(-\frac{E}{RT}\right)dT$$

Performing a change of variable with the following non-dimensional parameter $\xi = E/(RT)$, then

$$g(\alpha) = \frac{A_\alpha}{\beta} \frac{E_\alpha}{R} p\left(\frac{E}{RT}\right) \text{with} \ \ p(\nu_\alpha) : \ = \int_{\nu_\alpha}^\infty \frac{1}{\xi^2}\exp(-\xi)d\xi \tag{2}$$

or

$$\log[g(\alpha)] = \log\left[\frac{A_\alpha E}{R}\right] - \log\beta + \log\left[p\left(\frac{E}{RT}\right)\right] \tag{3}$$

where $g(\alpha)$ is known as the reaction model, and $\log z$ denotes natural logarithm of z.

2.2.2. Flynn-Wall-Ozawa (FWO) method

The FWO method [40] is normally applied to calculate the activation energy, which is based on TGA tests at heating constant rates. Then, the natural logarithm of the decomposition fraction is relating to the reciprocal of the absolute temperature, obtaining a linear function where its slope is proportional to the activation energy. Subsequently, Doyle's approximations algorithm was used in Eq. (3) [41] then obtaining the following equation

$$\ln \beta = \ln\left[\frac{A_\alpha E}{Rg(\alpha)}\right] - 5.331 - 1.052 \frac{E}{RT}.$$

2.2.3. Kissinger-Akahira-Sunose (KAS) method

The KAS is a differential method based on the Arrhenius formulation [42, 43]. It is deduced from this method that for a given conversion degree, the logarithm of the heating rate over the square of absolute temperature vs the reciprocal of the absolute temperature is a linear function. In other words, the slope is proportional to the activation
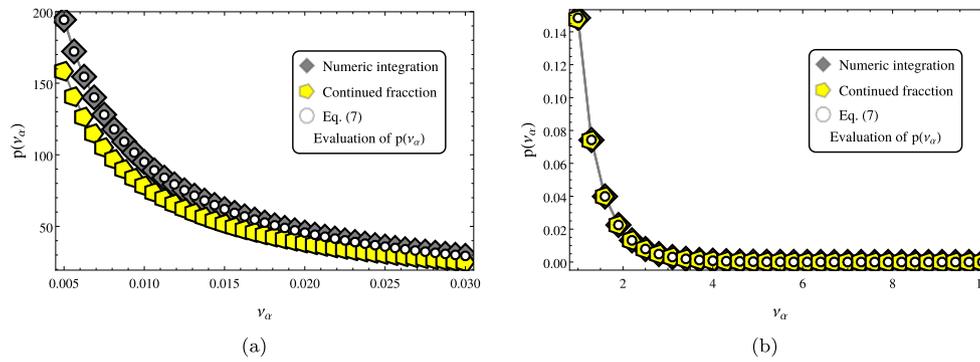
Fig. 1. Evaluation of the integral $p(\nu_\alpha)$ by using different methods. (a) The truncated continued fraction of five terms fails for small values of ν_α. (b) However, the continued fraction is good for $\nu_\alpha > 1$ where truncated 10-terms Taylor series can fail. White open dots correspond to Eq. (7) which is in agreement with numerical evaluation for positive real values of ν_α.

energy. To apply this technique is not required to know accurately the thermal decomposition mechanism [44]. Having manipulated the equation Eq. (3) and the Coats - Redfern [45] method which is expressed as follows

$$\log\left(\frac{\beta}{T^2}\right) = \log\left[\frac{A_\alpha R}{Eg(\alpha)}\right] - \frac{E}{RT} \text{ where } p\left(\frac{E}{RT}\right) \approx \left(\frac{RT}{E}\right)^2 \exp\left(-\frac{E}{RT}\right).$$

2.2.4. Friedman method

In this method, the activation energy uses the variation of conversion fraction regarding the temperature at a given heating rate and at a certain temperature. Thus, rearranging and applying natural logarithm in Eq. (1) it is obtained the following result

$$\log\left(\beta\frac{d\alpha}{dT}\right) = \log[A_\alpha f(\alpha)] - \frac{E}{RT}.$$

2.2.5. Vyazovkin method

The idea behind the FWO, KAS, and Friedman methods is to find the activation energy $E = E(\alpha)$ by plotting $\log\beta$, $\log(\beta/T^2)$ and $\log(\beta d\alpha/dT)$ vs the inverse of the temperature T^{-1} respectively. These plots are built for a fixed value of α and different values of heating rates β. Typically, it is obtained a straight line independently of the method used for each conversion grade, then the activation energy is obtained from its slope. Another strategy is described in the Vyazovkin's method. We start by considering the integral form of the reaction model

$$g(\alpha) = \int_0^\alpha \frac{d\alpha}{f(\alpha)} = \frac{A_\alpha}{\beta} I(E_\alpha, T) \text{ where } I(E_\alpha, T) = \int_0^T \exp\left(-\frac{E_\alpha}{RT}\right) dT. \quad (4)$$

Let us suppose that we performed M experiments with the following heating rates $\beta_1, \beta_2, ..., \beta_M$. If α and $g(\alpha)$ does not change when changing the temperature program then

$$g(\alpha) = \frac{A_\alpha}{\beta_i} I(E_\alpha, T_{\alpha,i}) \ i \in \mathscr{D}_M \quad (5)$$

where $\mathscr{D}_M := \{1, ..., M\}$ and $T_i(t) = T_{0i} + \beta_i t$. Now Eq. (5) is equivalent to

$$\frac{A_\alpha}{\beta_i} I(E_\alpha, T_{\alpha,i}) = \frac{A_\alpha}{\beta_j} I(E_\alpha, T_{\alpha,j})$$

for any i and j in $\mathscr{D}_M$, therefore

$$\frac{\beta_j I(E_\alpha, T_{\alpha,i})}{\beta_i I(E_\alpha, T_{\alpha,j})} = 1$$

applying a double sum over mixing all the possible different experiments, then

$$\sum_{\substack{i=1 \\ i\neq j}}^{M} \sum_{\substack{j=1 \\ i\neq j}}^{M} \frac{\beta_j I(E_\alpha, T_{\alpha,i})}{\beta_i I(E_\alpha, T_{\alpha,j})} = \sum_{\substack{i=1 \\ i\neq j}}^{M} \sum_{\substack{j=1 \\ i\neq j}}^{M} 1 = M(M-1)$$

This can be written as $\Phi_M(E_\alpha, \alpha) = 1$ with

$$\Phi_M(\varepsilon, \alpha) = \frac{1}{M(M-1)} \sum_{\substack{i=1 \\ i\neq j}}^{M} \sum_{j=1}^{M} \frac{\beta_j I(\varepsilon, T_{\alpha,i})}{\beta_i I(\varepsilon, T_{\alpha,j})}. \quad (6)$$

In general, the strict equality $\Phi_M(E_\alpha, \alpha) = 1$ cannot be reached because the temperature measurements have some experimental error. Nevertheless, the difference between both sides of Eq. (6) can be minimized by finding the value of E_α where $\Phi_M(\varepsilon, \alpha)$ has a global minimum $\varepsilon^*(\alpha)$, this is

$$\Phi_M : \mathscr{E} \to \mathbb{R} \text{if } (\forall \varepsilon \in \mathscr{E}) \ \Phi_M(\varepsilon^*(\alpha), \alpha) < \Phi_M(\varepsilon, \alpha)$$

for a given value of $\alpha \in [0, 1]$ where $\mathscr{E}$ is a range of possible expected energies per mol, in other words, the real positive numbers, but it can be reduced to a plausible expected activation energies per mol in the experiment. In general, we expect that global minimum $\varepsilon^*(\alpha) \to E_\alpha$ as we perform a large number M of experiments. It is necessary to evaluate the I-integral in Eq. (6), for this aim, it is feasible to use an algorithm to evaluate the integral numerically. In this study we evaluated Eq. (6) by using a combination of series expansions and continued fractions. It is necessary to compute multiple times the integral defined in Eq. (4) in order to evaluate $\Phi_M(\varepsilon, \alpha)$. This problem is very well known, and there are techniques to compute I [46].

It is convenient to define $\xi = E/(RT)$ then

$$I(E_\alpha, T) = \frac{E_\alpha}{R} p(\nu_\alpha) \text{with } p(\nu_\alpha) = \int_{\nu_\alpha}^{\infty} \frac{1}{\xi^2} \exp(-\xi) d\xi$$

integrating by parts

$$p(\nu_\alpha) = \frac{1}{\nu_\alpha} \exp(-\alpha) - \int_{\nu_\alpha}^{\infty} \frac{1}{\xi} \exp(-\xi) d\xi$$

second term in the right is the exponential integral $E_1(z)$ given by $E_1(z) = \int_z^\infty \exp(-\xi) d\xi$, then we may use the following continued fraction [47].

$$E_1(z) = \cfrac{\exp(-z)}{z+1-\cfrac{1}{z+3-\cfrac{4}{z+5-\cfrac{9}{z+7-\cfrac{15}{z+9-\cfrac{24}{z+11-\cfrac{35}{z+13-\cfrac{46}{z+15-\cdots}}}}}}}}$$

to compute the exponential integral. If the value of z is large, the previous continued fraction gives a good approximation by taking few fractions. However, if $z < 1$, it is advantageous to us Taylor expansion $\exp(-\xi) = \sum_{n=0}^{\infty} \frac{(-1)^n}{n!} \xi^n$ around $z = 0$, this enables to write

Table 1
Proximate, lignocellulosic and ultimate analysis of the SW.

Proximate analysis		Ultimate analysis	
		C %	44.52
Moisture %	10.10	H %	6.03
Volatiles %	79.86	N %	0.78
Ash %	1.20	O %	48.38
FC %	8.84	S %	0.59
		HHV (kJ/kg)	187040
Lignocellulosic Analysis		DRY HHV (kJ/kg)	20845
Cellulose %	34.43	DAF HHV (kJ/kg)	21127
Hemicellulose %	13.05	Empirical formula	$CH_{1.62}N_{0.015}O_{0.82}S_{0.0024}$
Lignine %	41.89	Enthalpy formation (kJ/mol)	-128455

$$E_1(z) = -\gamma - \log z - \sum_{n=1}^{\infty} \frac{(-1)^n}{n!n} \xi^n.$$

The ratio of convergence of the Taylor expansion for the exponential function is infinite. However, the Taylor series representation of $E_1(z)$ is an altering series, so we need a lot of terms to compute properly $E_1(z)$ as z increases. In practice, it is advisable to combine the Taylor series and the continued fraction to $p(\nu_\alpha)$ as it is shown in Eq. (7). In Fig. 1 we show a comparison between numerical integration and Eq. (7) by using 5-terms in the continuous fraction and truncating the Taylor series up to 10-terms.

$$p(\nu_\alpha) = \frac{e^{-\nu_\alpha}}{\nu_\alpha} + \gamma + \log z$$

$$+ \sum_{n=1}^{\infty} \frac{(-1)^n}{n!n} \nu_\alpha^n \text{ if } \nu_\alpha < 1 \text{ else } e^{-\nu_\alpha} \left(\frac{1}{\nu_\alpha} - \frac{1}{\nu_\alpha + 1 - \frac{1}{\nu_\alpha + 3 - \frac{4}{\nu_\alpha + 5 - \cdots}}} \right) \quad (7)$$

3. Results and discussion

3.1. Biomass characteristics

The sawmill waste SW samples underwent the proximate analysis, ultimate analysis, cellulose, hemicellulose, and lignin analysis. The results of the tests are shown in Table 1.

3.2. TGA results

This section presents the findings of TGA. In Fig. 2 is shown the volatile mass α of a SW sample as a function of the temperature between 25 °C and 1000 °C for five different heating rates $\{\beta_i\}_{i=1,\ldots,5} = \{10, 20, 30, 40, 50\}$ °C/min where m_1 y m_N are the residual mass at the beginning and final of the TGA respectively. This enables to compute the percentage of the residual mass as follows

$$\mathscr{P}_{res}(\alpha) := m(T)/m_1 = 1 + (m_N/m_1 - 1)\alpha.$$

Preceding studies have shown that a TGA curve can be analyzed as a function of four volatile compounds: moisture, cellulose, hemicellulose, and lignin [19, 36, 48, 49], and pyrolysis process of biomass is a simultaneous complex thermochemical conversion of cellulose, hemicellulose, and lignin [43]. Thus, i.e. at a heating rate $\beta = 20$ °C/min for the total volatile matter, water vaporized was 9%, the volatile matter between 200 °C and 400 °C by 76 % and for temperatures above 400 °C the volatile matter by 15 %. In our case, it was found a residual mass decrease by 8 % from 25 °C to 100 °C due to the vaporization of moisture contained in the biomass. On the other hand, for temperatures between 100 °C and 200 °C, there are no significant changes in the residual mass percentage but between 200 °C and 400 °C, the residual mass change is relevant due to the volatilization of the biochemical matter of SW.

Finally, for temperatures above 400 °C is found a slightly residual mass percentage change which means that the pyrolysis process for SW is presented between 200 °C and 400 °C mainly. According to the research performed in [20], TGA and DTG curves show a significant finding of cellulose, hemicellulose, and lignin decomposition. In the zone between 100 °C–200 °C it is usual to find volatilization of hemicellulose and lignin at a volatilization rate of 0.25 wt %/°C and null for the cellulose. Then, in

Fig. 3. DTG of SW.

(a)

(b)

Fig. 2. Volatile mass. (a) Degree of conversion α as a function of *T* for several heating rates. (b) Zoom for small values of α where black points at $(T_{p,i}^{(1)}, \alpha_{p,i}^{(1)})$ represents the different critical points for the *i*th heating rate. The yellow triangle and gray diamond are located at the average critical points $(<T_{p,i}^{(1)}>, <\alpha_{p,i}^{(1)}>)$ and $(<T_{p,i}^{(2)}>, \langle\alpha_{p,i}^{(2)}\rangle)$ respectively.
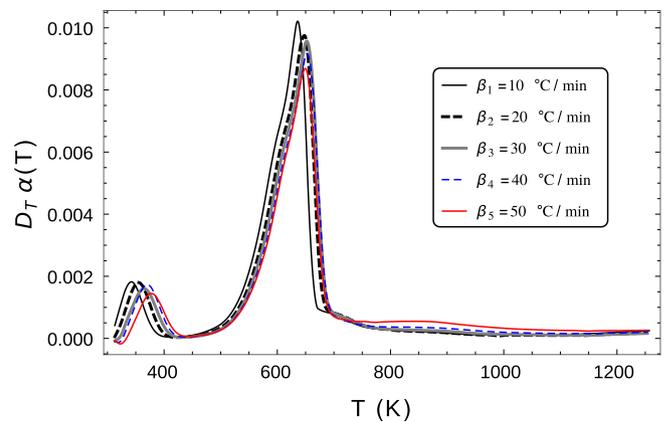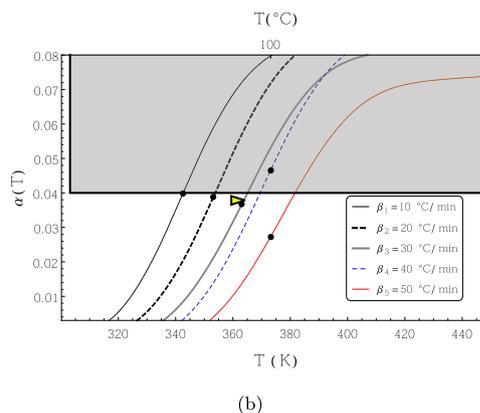
Table 2
Critical values for each heating rate.

i	$\beta_i\,[^\circ C/min]$	$T_{p,i}^{(1)}\,[K]$	$\alpha_{p,i}^{(1)}$	$T_{p,i}^{(2)}\,[K]$	$\alpha_{p,i}^{(2)}$
1	10	342.483	0.03972	637.483	0.6775
2	20	353.150	0.03879	643.150	0.6321
3	30	363.150	0.03676	653.150	0.6742
4	40	373.150	0.04660	653.150	0.6448
5	50	373.150	0.02726	653.150	0.6153

agreement with Fig. 2 is found a null volatilization of SW, it does not mean that there is no hemicellulose and lignin in the SW (see Table 1) but cellulose molecule chains round the most of lignin and hemicellulose molecules which do not allow their decomposition in the 100 °C–200 °C zone.

For the zone of 200 °C–400 °C is found the highest volatile mass amount and the highest rate of mass residual percentage per unit of time at a value of 22.14 %/min at a temperature of 375 °C and a heating rate of 30 °C/min (see Fig. 3) since most of hemicellulose composing the SW sample volatilizes at temperatures between 220 °C - 315 °C and most of the cellulose volatilizes at temperatures between 315 °C - 400 °C. For the zone between 400 °C - 1000 °C there is volatility rate lower than 0.09 wt % °C Fig. 3 because of lignin and hemicellulose within this temperature range which have a slow thermal decomposition since many chemical bonds and the structural mess. Thus, a slightly constant degradation carries out throughout the temperature domain. Since SW owns a high lignin amount (41,89 %), findings show that 15 % of SW volatile for the 400 °C–1000 °C zone Fig. 2 and at temperatures above 684 °C the volatility rate increased from 0.0087 wt %/°C to 0.04036 wt %/°C at 1000 °C for a heating rate of 10 °C/min (Fig. 3). The above mentioned occurred because lignin is composed by aromatic rings mainly which are broken at temperatures above 700 °C [50]. Furthermore, In Fig. 3 it is also possible to locate the critical temperatures where phase transitions of the different compounds of the biomass take place. For instance, there are zones where peaks occur for each heating rate β_i shown in Table 2. Thus, there are two $\mu = 1, 2$ sudden responses of α as temperature is increased, and they are located at $T_{p,i}^{(\mu)}$ for a given heating rate β_i. The corresponding critical values in the α-axis are $\alpha_{p,i}^{(\mu)} := \alpha(T_{p,i}^{(\mu)})$, and the average position is

$$\left\langle \left(T_p^{(\mu)}, \alpha_p^{(\mu)} \right) \right\rangle = \frac{1}{M} \sum_{i=1}^{M} \left(T_{p,i}^{(\mu)}, \alpha_{p,i}^{(\mu)} \right).$$

The corresponding average positions of both peaks for the current empirical data were located at $\langle (T_p^{(1)}, \alpha_p^{(1)}) \rangle = (361.017K, 0.03783)$ and $\langle (T_p^{(2)}, \alpha_p^{(2)}) \rangle = (648.017K, 0.6488)$. These points are plotted respectively as yellow and gray symbols in Fig. 2. As we mentioned before, it is expected that first critical temperature with average equals to $< T_p^{(1)} > = 361.017K = 87.867°C$ corresponds to the moisture contained in the

biomass, where such value should be near to the average boiling point of water at the corresponding pressures inside the TGA chamber. On the other hand, the second mean critical temperature $< T_p^{(2)} > = 648.017K = 374.867°C$ should corresponds to cellulose.

3.2.1. Activation energy

Discrete experimental data used to build the α vs T curve in Fig. 2 was also employed to construct the inverse function $T = T(\alpha)$ via a linear interpolation for any real value of α in $[0, 1]$ for each heating rate. Then, a short code was written in order to compute a standard linear regression according to KAS, FWO and Friedman methods, enabling to compute the activation energy $E = E(\alpha)$ for any real value of α from the slopes of the corresponding linear regressions automatically.

In Figs. 4 and 5 are shown the dependence on $\ln\beta$, $\ln(\beta/T^2)$ and $\ln(\beta d\alpha/dT)$ with the reciprocal of temperature. Each point in these plots represents a heating rate in $\{\beta_i\}_{1 \le i \le 5} = \{10, 20, 30, 40, 50\}$ °C/min at specific value of α. In particular, a hundred of values of α equally separated in $[0, 1]$ were selected in order to explore the linear fit proposed for each isoconversional method. In the data analysis, two regions were identified in $[0, 1]$ for the following α values

$$\chi_I = \{\alpha : 0 < \alpha < 0.04\} \text{ and } \chi_{II} = \{\alpha : 0.2 < \alpha < 0.7\}$$

where errors associated with the linear regressions obtained from the KAS, FWO, and Friedman methods are small as shown in Fig. 5-(b). The values of α not belonging to $\chi_I \cup \chi_{II}$ are represented as shaded regions where error of the r^2-coefficient is large. As a convention, the shaded regions in Fig. 5-(b) correspond to the same ones shown in another plot of the current document.

On Fig. 6-(a), the results obtained from the Vyazovkin by evaluating Eq. (6) with $M = 5$ temperature programs are shown. At first, an interpolation $\tilde{T}_i(\alpha)$ of the experimental data was performed in order to obtain the temperature as a function of α for each heating rate β_i. As done with the previous methods (FWO, KAS and Friedman), a short computer program was written to read data from M interpolated temperature functions (each one corresponding to a given heating rate) for a hundred of real values of α raging from 0 to 1. The program evaluated Eq. (6) by using Eq. (7) for a given value of α. The minimum value of each function $\Phi_M(\varepsilon, \alpha)$ was found with a standard Newton's method. Then, a convex curve with a single minimum was obtained. Once the minima $\varepsilon^*(\alpha) = E_\alpha$ were located, $\Phi_M(\varepsilon^*(E_\alpha, \alpha)) - 1$ was plotted in order to determine the interval of validity of the experimental data as shown in Fig. 6-(b). Since Φ_M was normalized, then it is expected that $\Phi_M(E_\alpha, \alpha) - 1$ tend to zero if the error associated to E_α is small. Thus we use $\Phi_M(E_\alpha, \alpha) - 1$ to estimate the range of validity of the energy computation (see Fig. 6-(b)). Thereby, this straightforward test suggests to pick those activation energies found within the interval $0.25 < \alpha < 0.7$ since the energies outside may have considerable error. As expected, the r^2-coefficient obtained from FWO, KAS and Friedman methods are comparable with those in $\Phi_M(\varepsilon^*(E_\alpha, \alpha)) - 1$ (see shaded regions in Figs. 5-(b) and 6-(b)).
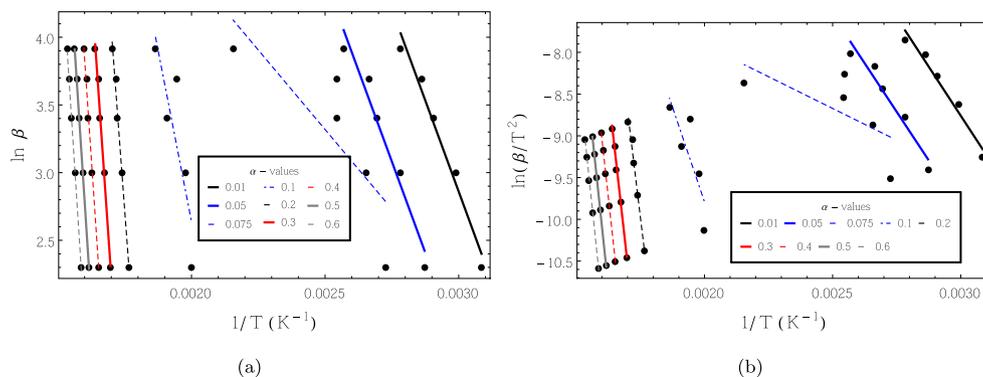
Fig. 4. Linear regression. (a) FWO method and (b) KAS method.
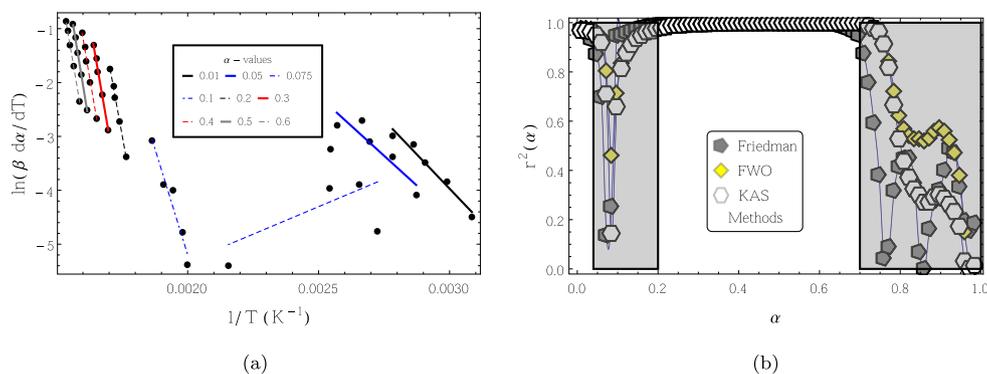
Fig. 5. Linear fit and estimated error. (a) Linear regression obtained with the Friedman method. (b) r^2-coefficient associated to linear regressions of FWO, KAS and Freidman methods. Lines connecting symbols are only to guide the eye.
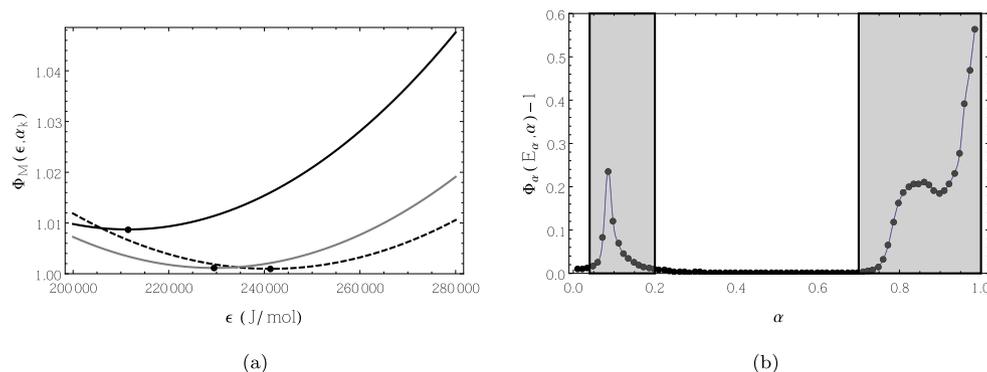
Fig. 6. (a) Evaluation of Eq. (6) for $\alpha_1 = 0.2$, $\alpha_2 = 0.5$ and $\alpha_3 = 0.7$ corresponding to the black-solid, black-dashed and gray-solid lines respectively. (b) Plot of $\Phi_M(\varepsilon, \alpha) - 1$ vs α evaluated at the their global minima $\varepsilon^*(\alpha) = E_\alpha$. Note that the error regions of $\Phi_M(\varepsilon, \alpha) - 1$ match with those predicted by r^2 in Fig. 5-(b).
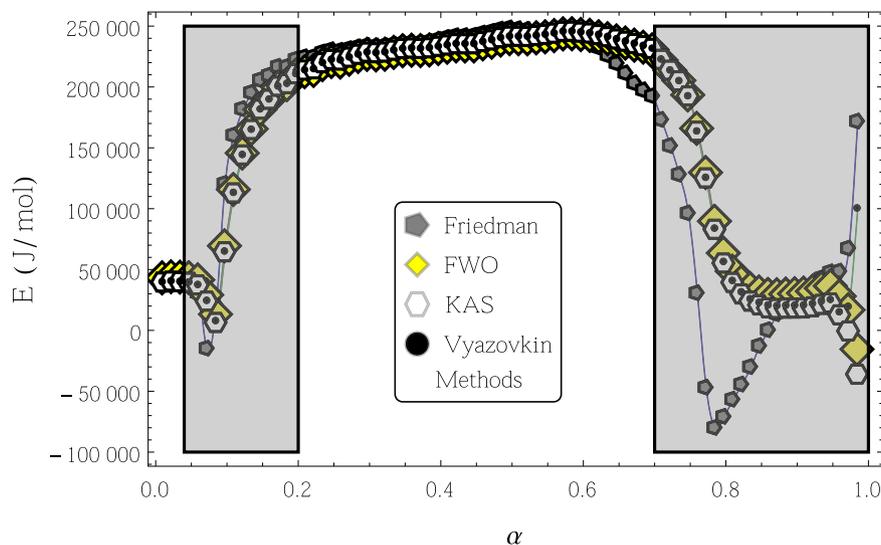
Fig. 7. Activation energy as a function of the degree of conversion in the interval $0 \leq \alpha \leq 1$. The shaded region represents the intervals where estimated errors are significant for the four isoconversional methods (see Figs. 5 and 6-(b)). Lines connecting symbols are only to guide the eye.

In Fig. 7 is shown the activation energy $E = E(\alpha)$ computed with the KAS, FWO, Friedman, and Vyazovkin methods for $\alpha \in [0, 1]$. The activation energies calculated with each method at a given conversion degree in $\chi_I \cup \chi_{II}$ are close each other. However, there is an important deviation observed regarding to the activation energy computed through the Friedman method in the interval $0.6 < \alpha < 0.7$ (see Figs. 7 and 8). It must be highlighted that Friedman method depends on the evaluation of

$d\alpha/dT$, while the others employed in the current work do not. Then regions where the numerical evaluation of such derivative has an important error may introduce relevant deviation on the activation energy computed via Friedman Method. As in our case study, the highest variation of $\alpha = \alpha(T)$ occurs in the region $0.6 < \alpha < 0.7$ where the value of α associated to the mean critical temperature $\langle T_p^{(2)} \rangle = 648.017K$ is $\langle \alpha_p^{(2)} \rangle = 0.6488$. It is expected that results $E(\alpha)$ obtained from Friedman method
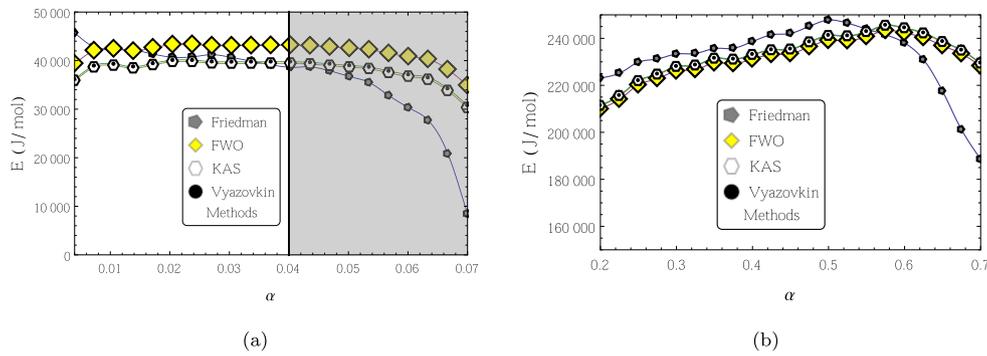
Fig. 8. Activation energy in the regions (a) χ_I and (b) χ_{II}. Lines connecting symbols are only to guide the eye.

are not suitable around $\langle \alpha_p^{(2)} \rangle$ since there are not enough experimental data near $\langle T_p^{(2)} \rangle$ to compute properly the derivative of such peak.

In general, the mean activation energy would not be an adequate result because biomass pyrolysis is a complex thermochemical process due to the diverse compounds and structures that constitute most of biomasses. Activation energy is commonly defined as the minimum energy amount to begin a reaction. For the biomass analyzed in this study to be used in pyrolysis processes, according to the Fig. 7, for FWO, KAS and Vyazovkin methods the maximum activation energy occurs at $\alpha^* = 0.587$. The energy increased at a rate of 85.57 (kJ/mol)/(kg/kg) in the interval $[0.2, \alpha^*]$ and it decreased at a mean rate of -130.85 (kJ/mol)/(kg/kg) from α^* to $\alpha = 0.7$. At α^* the activation energy is maximum because of the breakdown of hemicellulose and many endothermic-heterogenous reactions occurring around this value where yielding volatile matter products such as CO and CO_2 for SW. Generation of volatiles continues up to $\alpha = 0.7$ but the $E(\alpha)$ is lower because more heat is available in the environment due to the starting of exothermic reactions by the breaking of glycosidic linkages of polysaccharide producing blends of levoglucosan, oligosaccharides, and anhydrides as tar fraction [51]. Many complex chains compose biomass which surround cellulose, hemicellulose, and lignin avoiding the breaking bonds. Hence, predicting the activation energy of any biomass as a function of the hemicellulosic composition could be a mistake. For instance, Kaur et al. [52] calculated that for $\alpha = [0.4; 0.5]$ (comparable temperatures) the activation energy for castor residues was 214.33 kJ/mol and 215.56 respectively; and compared to the current work (SW), its activation energy was 231.15 kJ/mol and 239.07 kJ/mol respectively. However, the cellulose and hemicellulose content is 38.42 % and 22.40 % compared with that of the current work, 34.32 % and 13.05 % respectively. Although the activation energy of SW is higher by 9 % compared to castor residues, the SW residual mass at 500 °C is by 20 % compared to by 30 % of castor residues. Thus, SW remains suitable to be converted into value-fuel products.

3.3. Estimation of the reaction function

The reaction function can be written from the kinetic equation Eq. (1) as follows

$$f_i(\alpha) = \beta_i \frac{d\alpha}{dT}\Big|_{T=T_i(\alpha)} \frac{1}{A_\alpha(\beta_i)} \exp\left[\frac{E(\alpha)}{RT_i(\alpha)}\right]. \tag{8}$$

The pre-exponential factor can be estimated from

$$A_\alpha(\beta) = \frac{\beta E}{RT_p^2} \exp\left(\frac{E}{RT_p}\right) \tag{9}$$

where T_p is the peak temperature which is placed at the highest point in the $d\alpha/dT$ vs. T curve at a specific heating rate, k_B and h are the Boltzmann and Planck constant respectively. Eq. (9) is useful to calculate the pre-exponential factor when the activation energy profile does not have a large variation with α. However, in general, the pre-exponential

factor is another unknown. In principle, the function $f(\alpha)$ should be independent of the temperature program used, this is $f = f_1 = f_2 \cdots = f_M$. By virtue of this independence and Eq. (9) then

$$f(\alpha) = \frac{R}{ME(\alpha)} \sum_{j=1}^{M} T_{p,j}^2 \frac{d\alpha}{dT}\Big|_{T=T_j(\alpha)} \exp\left[\frac{E(\alpha)}{R}\left(\frac{1}{T_j(\alpha)} - \frac{1}{T_{p,j}}\right)\right] \tag{10}$$

Rigorously speaking, Eq. (9) may be used only in the case where the activation energy is a constant, or $E = E(\alpha)$ does not change substantially. Additionally, Eq. (9) assumes a first-order kinetics. In other words, we may use Eq. (10) to check if the reaction function $f = f_{HK}$ fits with a homogeneous kinetics, where

$$f_{HK}^{(n)}(\alpha) = (1 - \alpha)^n$$

and $n = 1$ for a first-order model. There are other approaches where it is assumed that pre-exponential factor $A = A(\alpha)$ is a constant, then the reaction function could be estimated as follows

$$f_{approx}(\alpha) = \frac{1}{AM} \sum_{j=1}^{M} \beta_i \frac{d\alpha}{dT}\Big|_{T=T_j(\alpha)} \exp\left[\frac{<_E}{RT_j(\alpha)}\right]$$

where

$$\langle E \rangle_\chi = \frac{1}{\alpha_2 - \alpha_1} \int_{\alpha \in \chi} E(\alpha) d\alpha \tag{11}$$

is the average of the energy in a given interval e.g. $\chi = [\alpha_1, \alpha_2] \in \mathbb{R}$. This approach usually works when the activation energy does not have a large variation in χ.

In the current study we preferred to compute the following quantity

$$Z(\alpha) = f(\alpha)g(\alpha)$$

since this approach avoids the computation of the pre-exponential factor and consequently any assumption behind it when the reaction function is estimated. Using the Eqs. (8) and (2) then

$$Z_i(\alpha) = f_i(\alpha)g_i(\alpha) = \beta_i \frac{d\alpha}{dT}\Big|_{T=T_i(\alpha)} \frac{1}{A_\alpha(\beta_i)} \exp\left[\frac{E(\alpha)}{RT_i(\alpha)}\right] \times \frac{A_\alpha(\beta_i)}{\beta_i} \frac{E_\alpha}{R} p\left[\frac{E(\alpha)}{RT_i(\alpha)}\right]$$

therefore

$$Z(\alpha) = \frac{E(\alpha)}{R} \frac{1}{M} \sum_{i=1}^{M} \frac{d\alpha}{dT}\Big|_{T=T_i(\alpha)} p\left[\frac{E(\alpha)}{RT_i(\alpha)}\right]. \tag{12}$$

The sum over different heating rates is frequently removed since β does not affect importantly the shape of the function $Z(\alpha)$, although here we decided to keep the average since its computation does not offer a great difficulty. The standard method corresponds to compute $Z(\alpha)$ with the experimental data and Eq. (12) in order to identify the best fitting with the theoretical models, some of these models are listed in Table 3. In

Table 3
Kinetic models.

Code	Reaction model	$f(\alpha)$	$g(\alpha)$	$z(\alpha) = f(\alpha)g(\alpha)$
P_4	Power law	$4\alpha^{3/4}$	$\sqrt[4]{\alpha}$	4α
P_3	Power law	$3\alpha^{2/3}$	$\sqrt[3]{\alpha}$	3α
P_2	Power law	$2\sqrt{\alpha}$	$\sqrt{\alpha}$	2α
$P_{\frac{2}{3}}$	Power law	$\dfrac{2}{3\sqrt{\alpha}}$	$\alpha^{3/2}$	$\dfrac{2\alpha}{3}$
D_1	1D-diffusion	$\dfrac{1}{2\alpha}$	α^2	$\dfrac{\alpha}{2}$
F_1	Mampel (first-order)	$1-\alpha$	$-\log(1-\alpha)$	$(\alpha-1)\log(1-\alpha)$
A_4	Avrami-Erofeev 4D-nucleation	$4(1-\alpha)(-\log(1-\alpha))^{3/4}$	$\sqrt[4]{-\log(1-\alpha)}$	$4(\alpha-1)\log(1-\alpha)$
A_3	Avrami-Erofeev 3D-nucleation	$3(1-\alpha)(-\log(1-\alpha))^{2/3}$	$\sqrt[3]{-\log(1-\alpha)}$	$3(\alpha-1)\log(1-\alpha)$
A_2	Avrami-Erofeev 2D-nucleation	$2(1-\alpha)\sqrt{-\log(1-\alpha)}$	$\sqrt{-\log(1-\alpha)}$	$2(\alpha-1)\log(1-\alpha)$
D_3	4D-diffusion	$\dfrac{3(1-\alpha)^{2/3}}{2(-\sqrt[3]{1-\alpha}-1)}$	$(1-\sqrt[3]{1-\alpha})^2$	$-\dfrac{3(\sqrt[3]{1-\alpha}-1)^2(1-\alpha)^{2/3}}{2(\sqrt[3]{1-\alpha}+1)}$
R_3	Contracting sphere	$3(1-\alpha)^{2/3}$	$1-\sqrt[3]{1-\alpha}$	$3(\alpha+(1-\alpha)^{2/3}-1)$
R_2	Contracting cylinder	$2\sqrt{1-\alpha}$	$1-\sqrt{1-\alpha}$	$2(\alpha+\sqrt{1-\alpha}-1)$
D_2	2D-diffusion	$-\dfrac{1}{\log(1-\alpha)}$	$\alpha+(1-\alpha)\log(1-\alpha)$	$\alpha-\dfrac{\alpha}{\log(1-\alpha)}-1$
F_2	second-order	$(1-\alpha)^2$	$\dfrac{1}{1-\alpha}-1$	$-(\alpha-1)\alpha$
F_3	third-order	$(1-\alpha)^3$	$\dfrac{1}{2}\left(\dfrac{1}{1-\alpha}-1\right)$	$\dfrac{1}{2}(\alpha-1)^2\alpha$
D_4	Ginstling-Brounshtein	$\dfrac{3}{2}\left(\dfrac{1}{\sqrt[3]{1-\alpha}}-1\right)$	$-\dfrac{2\alpha}{3}-(1-\alpha)^{2/3}+1$	$f(\alpha)g(\alpha)$

general, the theoretical function of $Z(\alpha)$ is obtained from the reaction function $f(\alpha)$ by integration

$$Z(\alpha) = f(\alpha)\int_0^\alpha \frac{1}{f(\alpha')}\,d\alpha'.$$

On Fig. 9 we show a normalized version of $Z(\alpha)$ in the interval χ_{II}, where the value of α_{ref} was selected as the middle point of region χ_{II}, this is $\alpha_{ref} = 0.45$. We used the corresponding values of activation energy obtained with the Vyazovkin method and Eq. (7) to evaluate the $Z(\alpha)$ in Eq. (12). The test with functions of Table 3 shows that best fitting is obtained when $f(\alpha)$ corresponds to a two-dimensional diffusion denoted as D_2. We also performed some tests of Eq. (10) and the first order model F_1, finding bad fittings (as it occurs with function $Z(\alpha)$ and the model F_1 in Fig. 9). This suggests that pre-exponential factor is not exactly the one predicted by Eq. (9). However, it is possible to use Eq. (1) to estimate the pre-exponential factor. If A is a function exclusively of the volatile mass, then

$$A(\alpha)f(\alpha) = \frac{1}{M}\sum_{i=1}^{M}\beta_i\frac{d\alpha}{dT}\bigg|_{T=T_i(\alpha)}\exp\left[\frac{E(\alpha)}{RT_i(\alpha)}\right].$$

According to the Z-master plot, the reaction is well described by a two-dimensional diffusion $f(\alpha) = -1/\log(1-\alpha)$, hence

$$\log[A(\alpha)] = \log\left\{-\frac{\log(1-\alpha)}{M}\sum_{i=1}^{M}\beta_i\frac{d\alpha}{dT}\bigg|_{T=T_i(\alpha)}\exp\left[\frac{E(\alpha)}{RT_i(\alpha)}\right]\right\}. \quad (13)$$

A plot of this function with the experimental data is shown in Fig. 10. We observed that experimental estimation of $\log A(\alpha)$ has an approximate linear dependence on α, then the pre-exponential factor estimated has an exponential behaviour as expected. Table 4 includes the computation of few values of A per heating rate by using Eq. (9).

In this study, the numerical values of the pre-exponential factor obtained with Eq. (9) and Eq. (13) provide different values because master plots suggest a two-dimensional diffusion D_2 mechanism instead of a first-order F_1 mechanism. Even if the F_1 and D_2 mechanism are far each other, we observed that Eq. (9) provides values of A in the range $[10^{17}, 10^{19}]s^{-1}$ in the interval $0.2 < \alpha < 0.6$ by using either the Vyazovkin or KAS methods whose $\beta = \beta_3$ (see the 4th and 5th columns in Table 4). Though Eq. (9) does not provide an exact values of A because a general

Table 4
Activation energy and pre-exponential factor for several conversion degrees via FWO, KAS, Friedman and Vyazovkin methods.

FWO method				
α	$E(\alpha)[J]$	r^2	$A_\alpha(\beta_3)$ Eq. (9) $[s^{-1}]$	$A(\alpha)[s^{-1}]$
0.2	209908.5604	0.97847	1.0866×10^{17}	8.38083×10^{17}
0.3	226049.3935	0.99335	2.2859×10^{18}	1.70023×10^{18}
0.4	231153.3223	0.99729	5.983×10^{18}	3.44929×10^{18}
0.5	239071.0445	0.99758	2.6592×10^{19}	6.99764×10^{18}
0.6	242321.4705	0.99696	4.904×10^{19}	1.41962×10^{19}
0.7	228237.7478	0.99717	3.4534×10^{18}	2.88001×10^{19}
KAS method				
α	$E(\alpha)[J]$	r^2	$A_\alpha(\beta_3)$ Eq. (9) $[s^{-1}]$	$A(\alpha)[s^{-1}]$
0.2	211234.7082	0.97648	1.3959×10^{17}	8.38083×10^{17}
0.3	227840.4204	0.99275	3.2042×10^{18}	1.70023×10^{18}
0.4	232942.4803	0.99705	8.3821×10^{18}	3.44929×10^{18}
0.5	241046.4497	0.99737	3.8574×10^{19}	6.99764×10^{18}
0.6	244276.0718	0.9967	7.0852×10^{19}	1.41962×10^{19}
0.7	229276.5062	0.99689	4.2004×10^{18}	2.88001×10^{19}
Friedman method				
α	$E(\alpha)[J]$	r^2	$A_\alpha(\beta_3)$ Eq. (9) $[s^{-1}]$	$A(\alpha)[s^{-1}]$
0.2	223049.8537	0.99122	1.2983×10^{18}	8.38083×10^{17}
0.3	233270.793	0.9967	8.917×10^{18}	1.70023×10^{18}
0.4	238637.7688	0.99833	2.4508×10^{19}	3.44929×10^{18}
0.5	247742.5753	0.9964	1.3605×10^{20}	6.99764×10^{18}
0.6	238037.6907	0.9977	2.1889×10^{19}	1.41962×10^{19}
0.7	188511.6526	0.9374	1.8977×10^{15}	2.88001×10^{19}
Vyazovkin method				
α	$E(\alpha)[J]$	$\Phi_M - 1$	$A_\alpha(\beta_3)$ Eq. (9) $[s^{-1}]$	$A(\alpha)[s^{-1}]$
0.2	211448.5159	0.0087363	1.4534×10^{17}	8.38083×10^{17}
0.3	228044.7919	0.0026908	3.33×10^{18}	1.70023×10^{18}
0.4	233150.6643	0.0010947	8.7175×10^{18}	3.44929×10^{18}
0.5	241255.7842	0.00097515	4.0125×10^{19}	6.99764×10^{18}
0.6	244489.5879	0.001223	7.3758×10^{19}	1.41962×10^{19}
0.7	229511.7373	0.0011456	4.3908×10^{18}	2.88001×10^{19}
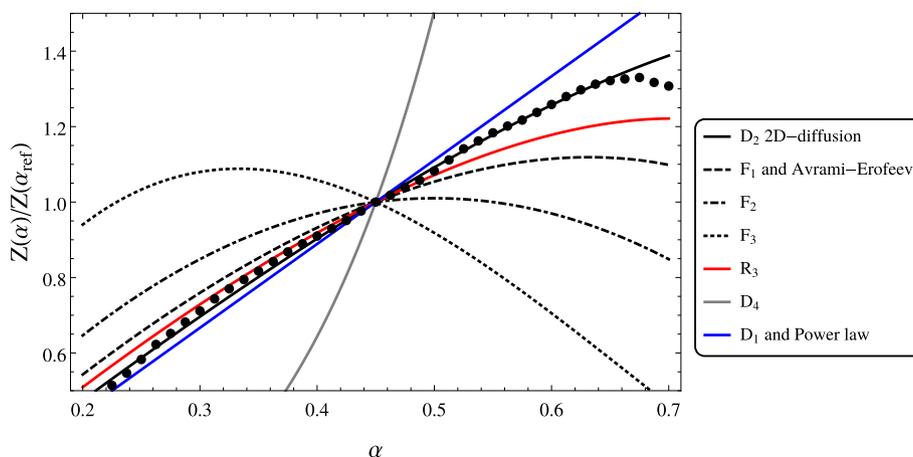
Fig. 9. Normalized plots of $Z(\alpha)$. The lines corresponds to theoretical functions and the black points are the values of $Z(\alpha)$ computed with Eq. (12) and the experimental data.
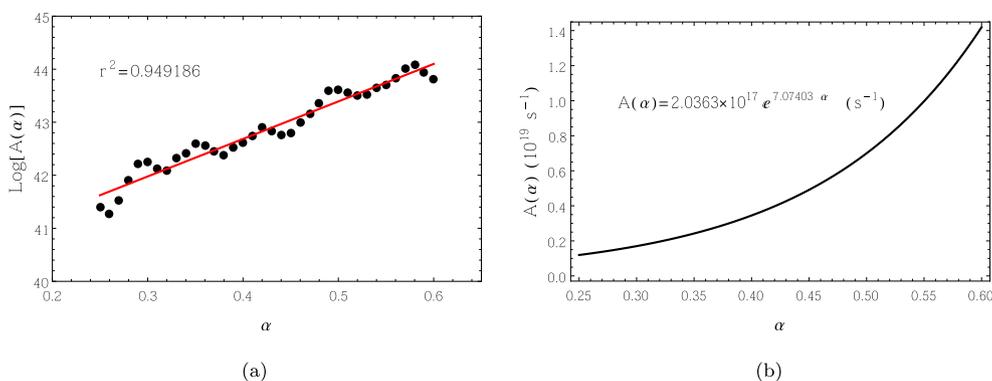
Fig. 10. Estimation of the pre-exponential factor. (a) Black dots correspond to Eq. (13) with the experimental data, and the solid line is the linear regression including the r^2 coefficient. (b) $A(\alpha)$ obtained from the linear regression.

formula would depend on $f(\alpha)$, it may give estimations of this factor with the same order of magnitude of other techniques like that one at Eq. (13).

4. Conclusions

In this document we found experimentally the degree of conversion α as function of T with several heating rates of the SW. Two fast changes of α at two temperatures $T_{p,i}^{(1)}$ and $T_{p,i}^{(2)}$ were located for each heating rate (see Table 2). These sudden changes of α at $T_{p,i}^{(1)}$ and $T_{p,i}^{(2)}$ are associated to phase transitions occurring in the SW. The first one is due to liquid/gas transition of the moisture, while the second one occurs when cellulose volatilizes. In principle, the FWO, KAS, Freidman and Vyazovkin methods are design under the assumption that the reaction $f = f(\alpha)$ does not change. This is just the behaviour observed in the region $\chi_I \cup \chi_{II} \subset [0, 1] \ni \alpha$ where the four isoconversional methods employed are in good agreement. On the other hand, these methods fail when $\alpha \notin \chi_I \cup \chi_{II}$ since errors associated to each method become important outside $\chi_I \cup \chi_{II}$. This situation of rapid growing of error occurs twice as T is increased and not too far from $T_{p,i}^{(1)}$ and $T_{p,i}^{(2)}$ as shown in Figs. 2, 5-(b) and 6-(b). Since the boiling process of moisture and the subsequent volatilization of cellulose are not necessary of the same nature, then $f(\alpha)$ can change between them and the isoconversional methods start to fail after $T_{p,i}^{(1)}$. A second region of considerable error occurs after $T_{p,i}^{(2)}$, but this is most related to the lack of reacting compounds in χ_{II}. Moreover, those regions where α changes slightly (this is $d\alpha/dT$ tends to zero), implies that $f(\alpha)$ tends to zero if $k(T)$ does not. This a consequence of the starting differential equation of the

kinetic theory. Then $f(\alpha)$ can change drastically as α runs from 0 to 1. For this reason is not very surprising that isoconversional methods have an important error when $d\alpha/dT$ is considerably small (see shaded regions in Fig. 2). Even if the model and analysis tools may give unexpected results in the error regions for the biomass studied here, the isoconversional methods used in this study are very useful because they give accurate results in $\chi_I \cup \chi_{II}$ where volatilization of cellulose occurs mainly and finding are useful for practical applications.

Experimental plots of $Z(\alpha) = f(\alpha)g(\alpha)$ matched with $Z_{D_2}(\alpha) = -\alpha - \alpha/\log(1-\alpha) - 1$, suggesting that reaction model behind the SW pyrolysis process is a two-dimensional diffusion. This enables us to compute the pre-exponential factor, finding a linear dependence between $\log A(\alpha)$ and α. Then in this study, it was possible to determine the kinetic triplet $E(\alpha), f(\alpha)$ and $A(\alpha)$ of the SW in the region χ_{II}.

The pyrolysis process for SW was found for a zone between 200° C–400° C since the volatile mass at 400^oC was by 75%. Moreover, in this zone was set the highest peak of degree conversion per temperature unit vs temperature $d\alpha/dT = 1.02 \times 10^{-2} (^o C)^{-1}$ at 359° C for $\beta = 10\,^o$C/min because both cellulose and hemicellulose decomposition rate is faster in the temperature zone above mentioned. Thus, the activation energy decreases when the conversion degree increases between 200^oC–400^oC for SW for the three non-isothermal isoconversional methods tested. The maximum activation energy was found at $\alpha^* = 0.587$, and its value $E(\alpha^*)$ according to FWO, KAS Friedman and Vyazovkin methods was 243.024, 245.038, 239.897 and 245.250 kJ/mol respectively. The mean energy in χ_{II} obtained by numerical integration of Eq. (11) and using the Vyazovkin method was $<_E = 233.744$ kJ/mol.

Declarations

Author contribution statement

Javier Bonilla, Robert Salazar, Manuel Mayorga: Conceived and designed the experiments; Performed the experiments; Analyzed and interpreted the data; Contributed reagents, materials, analysis tools or data; Wrote the paper.

Funding statement

This work was supported by Universidad ECCI, Colombia.

Competing interest statement

The authors declare no conflict of interest.

Additional information

No additional information is available for this paper.

References

[1] N. Cerone, F. Zimbardi, A. Villone, N. Strjiugas, E. Kiyikci, Gasification of wood and torrefied wood with air, oxygen, and steam in a fixed-bed pilot plant, Energy Fuels 30 (5) (2016) 4034–4043.

[2] X. Yuan, T. He, H. Cao, Q. Yuan, Cattle manure pyrolysis process: kinetic and thermodynamic analysis with isoconversional methods, Renew. Energy 107 (2017) 489–496.

[3] D. Mohan, C.U. Pittman Jr., P.H. Steele, Pyrolysis of wood/biomass for bio-oil: a critical review, Energy Fuel. 20 (3) (2006) 848–889.

[4] L. Wei, S. Xu, L. Zhang, C. Liu, H. Zhu, S. Liu, Steam gasification of biomass for hydrogen-rich gas in a free-fall reactor, Int. J. Hydrogen Energy 32 (1) (2007) 24–31.

[5] Z. Zhang, S. Pang, Experimental investigation of biomass devolatilization in steam gasification in a dual fluidised bed gasifier, Fuel 188 (2017) 628–635.

[6] J. Bonilla, G. Gordillo, Adiabatic fixed-bed gasification of colombian coffee husk using air-steam blends for partial oxidation, J. Comb. 2017 (2017).

[7] H. Chen, Applications of lignocellulose biotechnology in bioenergy. Biotechnology Of Lignocellulose, Springer, 2014, pp. 213–245.

[8] S.A. Gardezi, B. Joseph, F. Prado, A. Barbosa, Thermochemical biomass to liquid (btl) process: bench-scale experimental results and projected process economics of a commercial scale process, Biomass Bioenergy 59 (2013) 168–186.

[9] W.-H. Chen, B.-J. Lin, M.-Y. Huang, J.-S. Chang, Thermochemical conversion of microalgal biomass into biofuels: a review, Bioresour. Technol. 184 (2015) 314–327.

[10] A. Kumar, D. Jones, M. Hanna, Thermochemical biomass gasification: a review of the current status of the technology, Energies 2 (3) (2009) 556–581.

[11] S. Ren, H. Lei, L. Wang, Q. Bu, S. Chen, J. Wu, J. Julson, R. Ruan, Biofuel production and kinetics analysis for microwave pyrolysis of douglas fir sawdust pellet, J. Anal. Appl. Pyrolysis 94 (2012) 163–169.

[12] T. Kan, V. Strezov, T.J. Evans, Lignocellulosic biomass pyrolysis: a review of product properties and effects of pyrolysis parameters, Renew. Sustain. Energy Rev. 57 (2016) 1126–1140.

[13] A.V. Bridgwater, Review of fast pyrolysis of biomass and product upgrading, Biomass Bioenergy 38 (2012) 68–94.

[14] M.S. Ahmad, M.A. Mehmood, S.T.H. Taqvi, A. Elkamel, C.-G. Liu, J. Xu, S.A. Rahimuddin, M. Gull, Pyrolysis, kinetics analysis, thermodynamics parameters and reaction mechanism of typha latifolia to evaluate its bioenergy potential, Bioresour. Technol. 245 (2017) 491–501.

[15] F. Meng, J. Yu, A. Tahmasebi, Y. Han, H. Zhao, J. Lucas, T. Wall, Characteristics of chars from low-temperature pyrolysis of lignite, Energy Fuels 28 (1) (2013) 275–284.

[16] T. Yuan, A. Tahmasebi, J. Yu, Comparative study on pyrolysis of lignocellulosic and algal biomass using a thermogravimetric and a fixed-bed reactor, Bioresour. Technol. 175 (2015) 333–341.

[17] A.C.R. Lim, B.L.F. Chin, Z.A. Jawad, K.L. Hii, Kinetic analysis of rice husk pyrolysis using kissinger-akahira-sunose (kas) method, Procedia Eng. 148 (2016) 1247–1251.

[18] C. Quan, N. Gao, Q. Song, Pyrolysis of biomass components in a tga and a fixed-bed reactor: thermochemical behaviors, kinetics, and product characterization, J. Anal. Appl. Pyrolysis 121 (2016) 84–92.

[19] S.D. Stefanidis, K.G. Kalogiannis, E.F. Iliopoulou, C.M. Michailof, P.A. Pilavachi, A.A. Lappas, A study of lignocellulosic biomass pyrolysis via the pyrolysis of cellulose, hemicellulose and lignin, J. Anal. Appl. Pyrolysis 105 (2014) 143–150.

[20] H. Yang, R. Yan, H. Chen, D.H. Lee, C. Zheng, Characteristics of hemicellulose, cellulose and lignin pyrolysis, Fuel 86 (12-13) (2007) 1781–1788.

[21] M. Besson, P. Gallezot, C. Pinel, Conversion of biomass into chemicals over metal catalysts, Chem. Rev. 114 (3) (2013) 1827–1870.

[22] P. Gallezot, Conversion of biomass to selected chemical products, Chem. Soc. Rev. 41 (4) (2012) 1538–1558.

[23] H. Zabed, J. Sahu, A. Boyce, G. Faruq, Fuel ethanol production from lignocellulosic biomass: an overview on feedstocks and technological approaches, Renew. Sustain. Energy Rev. 66 (2016) 751–774.

[24] J. Lee, Biological conversion of lignocellulosic biomass to ethanol, J. Biotechnol. 56 (1) (1997) 1–24.

[25] J.B. Holm-Nielsen, T. Al Seadi, P. Oleskowicz-Popiel, The future of anaerobic digestion and biogas utilization, Bioresour. Technol. 100 (22) (2009) 5478–5484.

[26] D.P. Chynoweth, J.M. Owens, R. Legrand, Renewable methane from anaerobic digestion of biomass, Renew. Energy 22 (1-3) (2001) 1–8.

[27] P. Basu, Biomass Gasification, Pyrolysis and Torrefaction: Practical Design and Theory, Academic press, 2018.

[28] J.O. Akowuah, F. Kemausuor, S.J. Mitchual, Physico-chemical characteristics and market potential of sawdust charcoal briquette, Int. J. Energy Environ. Eng. 3 (1) (2012) 20.

[29] FAO, Forestry Production and Trade, 1999.

[30] M. Heydari, M. Rahman, R. Gupta, Kinetic study and thermal decomposition behavior of lignite coal, Int. J. Chem. Eng. 2015 (2015).

[31] S. Vyazovkin, A.K. Burnham, J.M. Criado, L.A. Pérez-Maqueda, C. Popescu, N. Sbirrazzuoli, Ictac kinetics committee recommendations for performing kinetic computations on thermal analysis data, Thermochim. Acta 520 (1-2) (2011) 1–19.

[32] S. Vyazovkin, Isoconversional Kinetics of Thermally Stimulated Processes, Springer, 2015.

[33] Product compositions and kinetics for rapid pyrolysis of cellulose, Ind. Eng. Chem. Process Des. Dev. 21 (3) (1982) 457–465.

[34] C. Koufopanos, N. Papayannakos, Modelling of the pyrolysis of biomass particles. studies on kinetics, thermal and heat transfer effects, Can. J. Chem. Eng. 69 (1991).

[35] A.K. Sadhukhan, P. Gupta, R.K. Saha, Modelling and experimental studies on pyrolysis of biomass particles, J. Anal. Appl. Pyrolysis 81 (2) (2008) 183–192.

[36] L. Burhenne, J. Messmer, T. Aicher, M.-P. Laborie, The effect of the biomass components lignin, cellulose and hemicellulose on tga and fixed bed pyrolysis, J. Anal. Appl. Pyrolysis 101 (2013) 177–184.

[37] S. Sobek, S. Werle, Solar pyrolysis of waste biomass: Part 1 reactor design, Renew. Energy 143 (2019) 1939–1948.

[38] H. Jouhara, Potential of pyrolysis processes in the waste management sector, Therm. Sci. Eng. Prog. 3 (2017) 171–197.

[39] Fast pyrolysis of biomass in a spouted bed reactor: wydrodynamics, heat transfer and chemical reaction, Renew. Energy 143 (2019) 1268–1284.

[40] J.H. Flynn, L.A. Wall, A quick, direct method for the determination of activation energy from thermogravimetric data, J. Polym. Sci. Part B: Polym. Lett. 4 (5) (1966) 323–328.

[41] C. Doyle, Estimating isothermal life from thermogravimetric data, J. Appl. Polym. Sci. 6 (24) (1962) 639–642.

[42] H.E. Kissinger, Variation of peak temperature with heating rate in differential thermal analysis, J. Res. Natl. Bur. Stand. 57 (4) (1956) 217–221.

[43] H.E. Kissinger, Reaction kinetics in differential thermal analysis, Anal. Chem. 29 (11) (1957) 1702–1706.

[44] M. Chao, W. Li, X. Wang, "Influence of antioxidant on the thermal–oxidative degradation behavior and oxidation stability of synthetic ester, Thermochim. Acta 591 (2014) 16–21.

[45] C. Graymore, © 1964 Nature Publishing Group, 1964.

[46] G. Senum, R. Yang, Rational approximations of the integral of the arrhenius function, J. Therm. Anal. Calorim. 11 (3) (1977) 445–447.

[47] P.-H. Tseng, T.-C. Lee, Numerical evaluation of exponential integral: theis well function approximation, J. Hydrol. 205 (1-2) (1998) 38–51.

[48] K. Raveendran, A. Ganesh, K.C. Khilar, Pyrolysis characteristics of biomass and biomass components, Fuel 75 (8) (1996) 987–998.

[49] V. Pasangulapati, K.D. Ramachandriya, A. Kumar, M.R. Wilkins, C.L. Jones, R.L. Huhnke, Effects of cellulose, hemicellulose and lignin on thermochemical conversion characteristics of the selected biomass, Bioresour. Technol. 114 (2012) 663–669.

[50] M. Zhai, X. Wang, Y. Zhang, P. Dong, G. Qi, Y. Huang, Characteristics of rice husk tar secondary thermal cracking, Energy 93 (2015) 1321–1327.

[51] Y. Xu, B. Chen, Investigation of thermodynamic parameters in the pyrolysis conversion of biomass and manure to biochars using thermogravimetric analysis, Bioresour. Technol. 146 (2013) 485–493.

[52] R. Kaur, P. Gera, M.K. Jha, T. Bhaskar, Pyrolysis kinetics and thermodynamic parameters of castor (ricinus communis) residue using thermogravimetric analysis, Bioresour. Technol. 250 (2018) 422–428.